Int. J. Electrochem. Sci., 9 **(2014)** 4574 - 4588

International Journal of
ELECTROCHEMICAL
SCIENCE
www.electrochemsci.org

Corrosion Behavior of X80 Pipeline Steel under Coupling Effect of Stress and Stray Current

Xinhua Wang, Xinghua Tang[*]*, Liwei Wang, Cui Wang, Zhenzhen Guo*

College of Mechanical Engineering and Applied Electronics Technology, Beijing University of Technology, Beijing, 100124, China.
[*]E-mail: txh-1110-163-com@163.com

Received: 25 March 2014 / *Accepted:* 4 May 2014 / *Published:* 19 May 2014

In this work, the coupling effect of stress and stray current on corrosion of X80 pipeline steel was investigated in soil-simulating solution by open circuit potential (OCP) and corrosion potential test, potentiodynamic polarization measurement and surface characterisation technique. A mathematical relationship between corrosion rate and yield strength, direct current (DC) stray current density was obtained through multiple linear regression. The results indicate that, the corrosion potential of X80 pipeline steel with and without superimposed DC stray current all shift negatively, and the corrosion rate increases with the enhancement of tensile stress in solution. Moreover, the above laws become increasingly obvious with DC stray current density form 0.5 to 3.5 mA/cm^2. Comparing with the stress, the effect of stray current on corrosion rate of X80 pipeline steel is more significant in elastic deformation. Mutation in corrosion potential and corrosion rate appeared when the strain reaches plastic deformation. This study provides important recommendations for pipeline safety design and operation, where the corrosion enhancement due to the coupling effect of stress and stray current should be considered.

Keywords: X80 pipeline steel, tensile stress, stray current, corrosion potential, corrosion rate

1. INTRODUCTION

With the fast development of industry and urbanization process, the global demand for oil and gas is rapidly increasing. This increase in demand means that a greater supply of resources is required over long distances that typically exist between the reservoirs and demand centres [1, 2]. The global trends for this sector of the petroleum and natural gas industry, point to the use of pipes with larger diameters and smaller wall thicknesses, operating under high pressure [3-5]. As is known [6-8], X80

pipeline steel is widely used in the transportation of oil and gas energy sources due to its high strength and excellent toughness.

In addition to hoop stress resulted from internal operating pressure, ground movement generates significant longitudinal strains on the in-service high-strength steel pipelines [9-11]. It has been established [12-14] that an applied stress/strain enhance corrosion of steel remarkably. Moreover, railway, urban rail DC traction power supply systems and ultra high voltage direct current (UHVDC) power transmission systems are often parallell to pipelines. Thus, DC currents would transfer between the soil and pipeline at the coating defects that could result in DC corrosion. In-service high-strength steel pipeline corrosion is often subjected synergism of stress and stray current. Howerve, previous studies [15-22] has been mostly focused on corrosion that stress, stray current or other single factor induced, little information available in literature about corrosion behavior of pipeline steel under coupling effect of stress and stray current. This paper focuses on the corrosion enhancement due to the coupling effect of stress and stray current, and provides important recommendations for pipeline safety design and operation.

In this work, X80 pipeline steel produced in China was used. The soil solution simulated a alkaline soil in Daqing City. OCP, potential of stray current-induced corrosion, polarization curve of X80 steel under tensile stress (hereinafter called "T_S") were measured, the influence law of stress on stray current-induced corrosion potential and corrosion rate of X80 pipeline steel was investigated combining with corrosion morphology.

2. EXPERIMENTAL

Specimens used in this study were cut from a sheet of in-service X80 steel pipe wall, with a chemical composition (wt.%) shown in Table 1. The mechanical properties at room temperature were measured with tensile strength of 620 MPa, yield strength (hereinafter called "Y_S") of 552 MPa and uniform elongation ratio of 15%.

Table 1. Chemical composition of X80 pipeline steel (wt.%).

C	Mn	P	S	Si	Nb	V	Ti	Cr	Ni	Al	Cu	Mo
0.06	1.89	0.007	0.002	0.26	0.06	0.005	0.01	0.025	0.23	0.042	0.13	0.27

The shape and size of specimen was shown in Fig.1. The sample surface was ground by emery paper from 150 to 2000 grit, and then rinsed with deionized water and degreased in acetone. The working surface of the sample was exposed to the soil-simulating solution; the other parts were covered by silicone rubber.

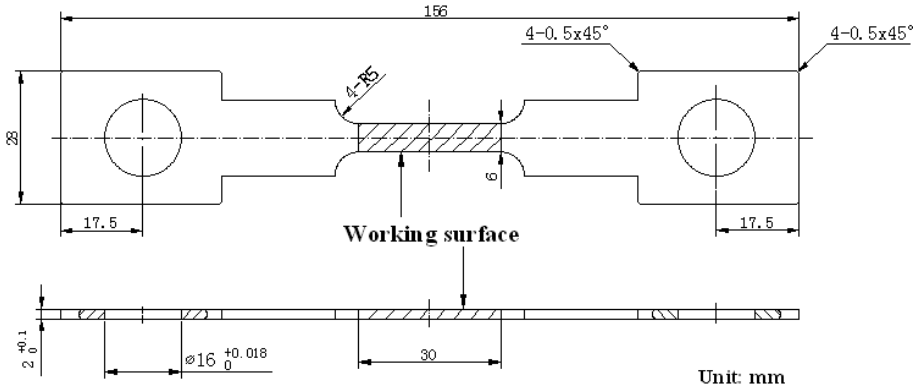

Figure 1. Schematic of X80 steel specimen for electrochemical measurement.

The sample was tested under different stress conditions (0%, 30%, 50%, 80%, 100%Y_S). The minimum cross-sectional area of the sample is 12 mm^2 (according to Fig. 1), and therefore we could calculate the actual stress specimens suffered are 0MPa, 165.6MPa, 276MPa, 441.6MPa, 552MPa, respectively. Area of specimen in contact with solution is 4.8cm^2, stray current density (hereinafter called "D_I") specimen suffered are 0.5, 1.0, 1.5, 2.0, 2.5, 3, 3.5 mA/cm^2, respectively, hereby, we could calculate the DC required for the experiment are 2.4, 4.8, 7.2, 9.6, 12, 14.4, 16.8 mA, respectively.

There are many high-strength steel pipelines in Daqing where important oil-producing area in China, meanwhile, this area is alkaline soil. Ionic concentrations and related parameters in Daqing soil as shown in table 2, table 3 shows reagents for preparing solution.

Table 2. Ionic concentrations and related parameters in Daqing soil.

pH	Conductivity	NO_3^-	Cl^-	$SO4^{2-}$	HCO_3^-	Ca^{2+}	Mg^{2+}	K^+	Na^+
9.19	0.20 mS/cm	0.084g	0.042g	0.138g	0.263g	0.092g	0.023g	0.003g	0.052g

Table 3. Simulated solution preparation table.

$CaCl_2$	NaCl	Na_2SO_4	$MgSO_4 \cdot 7H_2O$	KNO_3	$NaHCO_3$
0.084g	0g	0.109g	0.062g	0.086g	1.727g

All corrosion tests were carried out using the experimental platform (shown in Fig. 2). The experimental platform was mainly composed of the PC, Solartron electrochemical measurement system (1287 electrochemical interface and 1260A Impedance/Gain-Phase analyzer), excitation power, voltage amplifier, digital multimeter (DMM), stress loading system. Experimental platform physical graph as shown in Fig. 3. Among them, the stress loading system included excitation power, the DC signal isolators, DMM, mechanical parts.

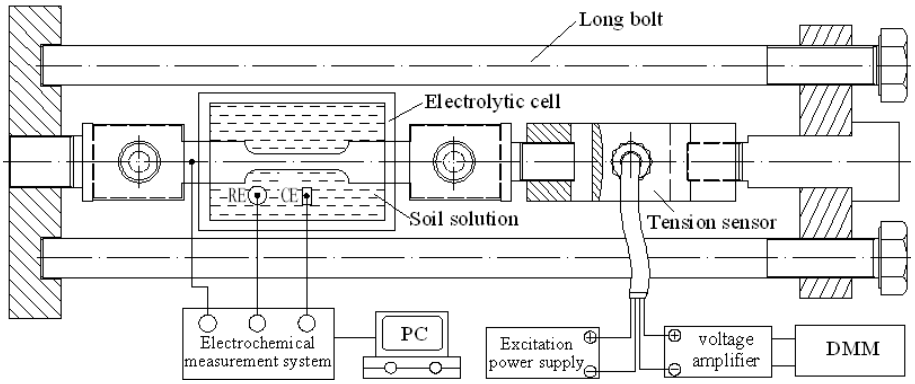

Figure 2. Schematic diagram of the experimental platform for corrosion of X80 steel under coupling effect of stress and stray current in Daqing simulated solution.

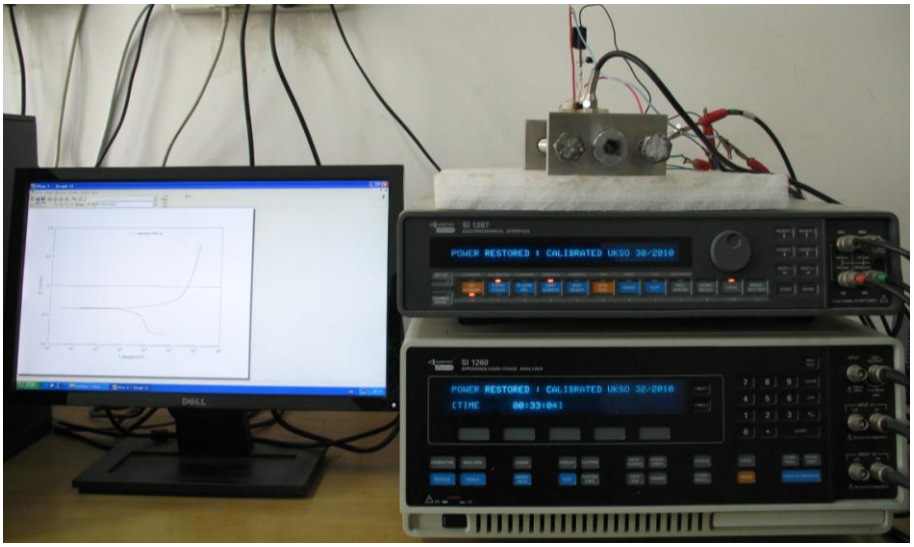

Figure 3. The experimental platform for corrosion of X80 steel under coupling effect of stress and stray current in Daqing simulated solution.

Before electrochemical measurement, rotating long bolt to generate tensile stress, DMM real-time displays values tension sensor obtained. Stop rotating long bolt until the desired stress. Electrochemical measurements were performed using the Solartron electrochemical system on a three-electrode cell, where the steel electrode was used as the working electrode (WE), a platinum sheet as the counter electrode (CE) and a saturated calomel electrode (SCE) as the reference electrode (RE).

3. RESULTS

3.1. The OCP under different stress conditions

Fig. 4 presents the OCP of X80 pipeline steel under different stress conditions in Daqing solution, it can be seen from the Fig. 4 that the OCP is shifted negatively gradually as stress increase.

According to the results in Fig. 4, the OCP of X80 steel under different stress conditions is processed to obtain the relationships curve of OCP with stress changes in Fig. 5. Wang et al. [22] suggested that the strain has a significant effect on the corrosion resistance of the X80 pipeline steel and low-strain also influences corrosion resistance; Ren et al. [23] found that the dominated process at the beginning of elastic deformation is stress accelerating corrosion of low carbon steel in 3.5 wt% NaCl solution; Xu et al. [24] reported that the effect of elastic stress/strain on corrosion of X100 steel is through its role in two aspects of the steel, i.e., electro-chemical potential and corrosion scale; Rao et al. [25] pointed out that when stressed, free corrosion potentia1 of LY12CZ aluminum alloy move negatively, the movement extent depend on the stress. We find that stress negatively correlated with the open-circuit potential in the elastic strain range from Fig. 5. Obviously, for the purposes of X80 pipeline steel, the influence law of stress on open circuit potential is similar with conclusions in paper [22-25]. From a thermodynamic point of view, the value of the electrode potential is directly related to the corrosion tendency of materials. The higher the electrode potential is, the less the corrosion tendency [22]. The corrosion resistance of X80 steel decrease as the stress increase.

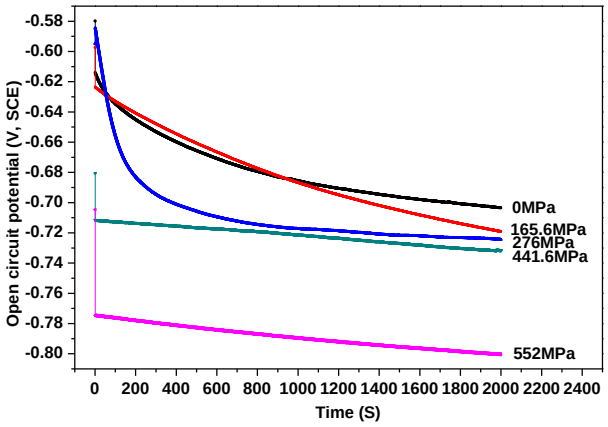

Figure 4. The open circuit potential (OCP) of X80 steel in Daqing soil solution under different tensile stress levels.

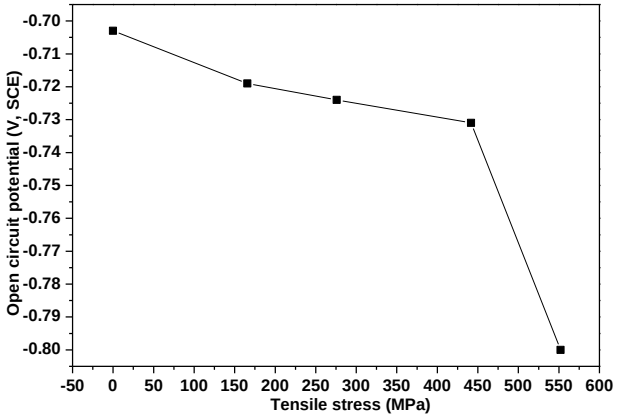

Figure 5. The relation curve between open circuit potential (OCP) and tensile stress of X80 steel in Daqing soil solution.

3.2. Potential changes under different DC stray current density and stress

Fig. 6 shows the potential of X80 steel under different DC stray current density when Ts are 0MPa (a), 165.6MPa (b), 276MPa (c), 441.6MPa (d), 552MPa (e), respectively.

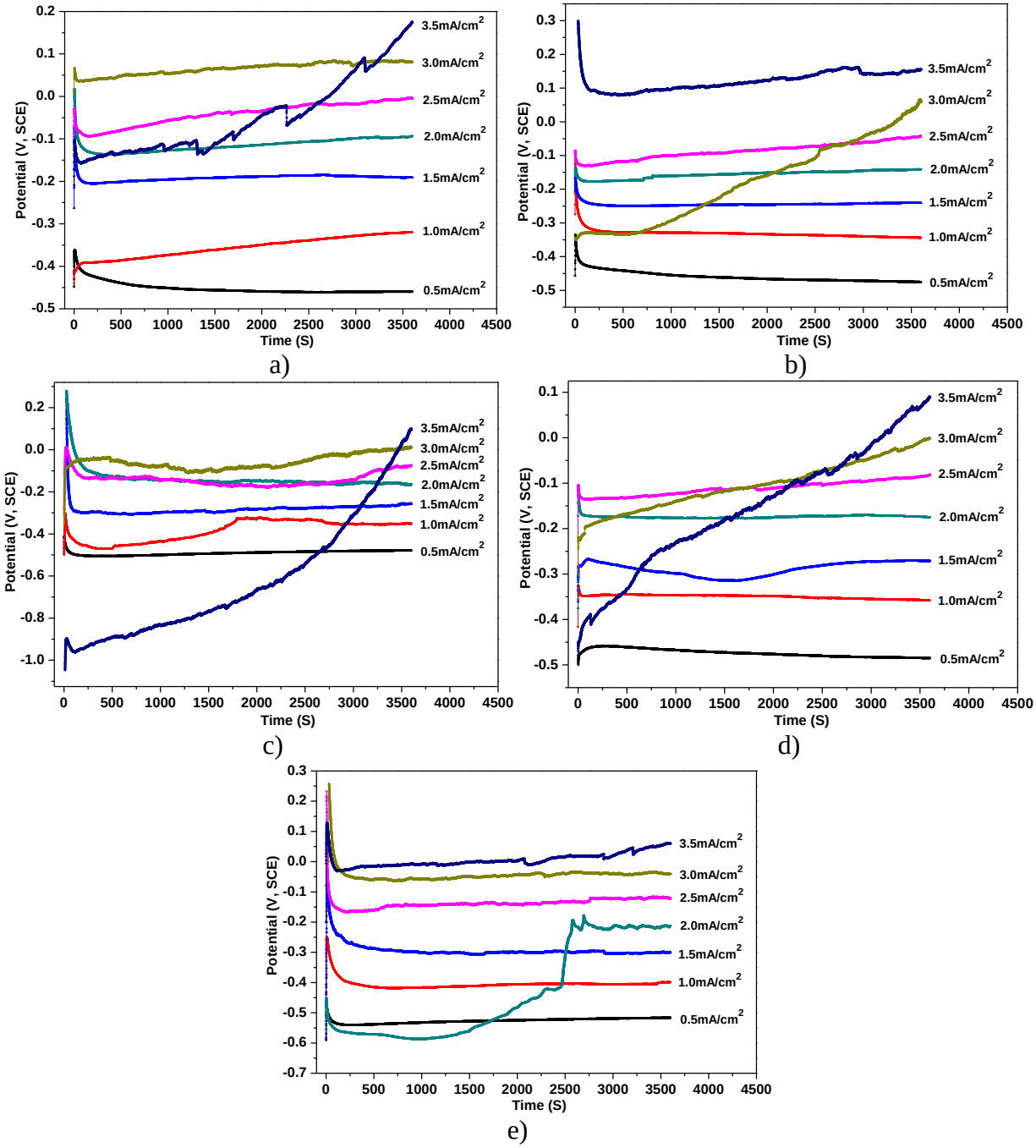

Figure 6. Potential of X80 steel under different DC stray current density when Ts are 0MPa (a), 165.6MPa (b), 276MPa (c), 441.6MPa (d), 552MPa (e), respectively.

It is seen that the corrosion potential of X80 pipeline steel shows a rising trend as stray current density increases. Extract from Fig. 6 that the potential value of X80 pipeline steel under different

stress and stray current density (as shown in table 4), and then draw the relationship diagram that stray current density and potential under different stress states as shown in Fig. 7.

Xu et al. [24] pointed out that an application of static elastic stress has very limited effect on the corrosion of X100 steel, while, plastic stress would ‘‘weaken’’ the corrosion scale by expanding its pores and increase the corrosion activity of the steel and thus. Cheng et al.[26,27] thought that the steady-state corrosion potential of X100 steel becomes more negative with the increase of pre-strain. We can see that the potential of X80 steel increases gradually as the stray current density increases, the stress reduces from Fig. 7.

Table 4. The potential of X80 pipeline steel under different stress and stray current density.

Ts (MPa)	0.5 mA/cm^2	1.0 mA/cm^2	1.5 mA/cm^2	2.0 mA/cm^2	2.5 mA/cm^2	3.0 mA/cm^2	3.5 mA/cm^2
0	-0.459	-0.320	-0.201	-0.103	-0.015	0.071	0.165
165.5	-0.475	-0.344	-0.240	-0.140	-0.043	0.049	0.145
273	-0.479	-0.352	-0.256	-0.165	-0.075	0.010	0.099
441.6	-0.485	-0.359	-0.271	-0.175	-0.082	-0.001	0.090
552	-0.516	-0.399	-0.310	-0.221	-0.131	-0.051	0.051

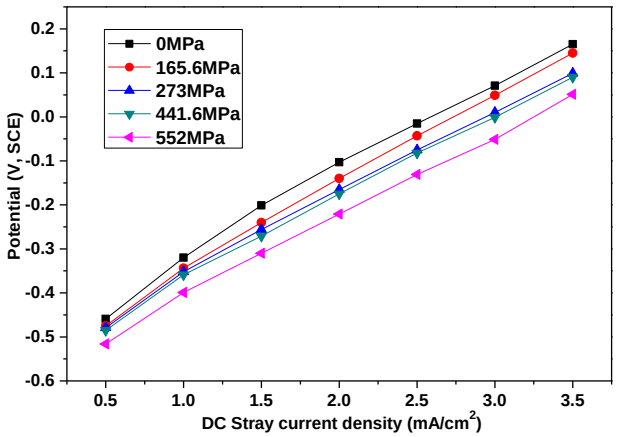

Figure 7. The relation curve between potential and DC stray current density of X80 pipeline steel in Daqing solution under different tensile stress levels.

3.3. Polarization curve under different stress levels

Fig. 8 shows polarization curve of X80 steel in Daqing solution under different stress levels. It is pointing out that corrosion current density increases and corrosion potential is shifted negatively with the increase of Ts.

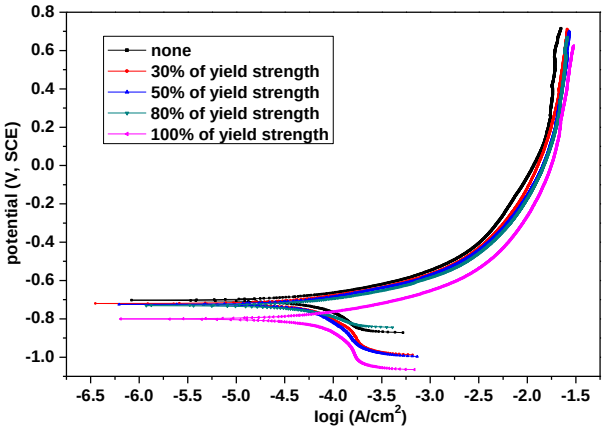

Figure 8. Polarization curve of X80 steel in Daqing solution under different stress levels.

Bonora et al. [28] noted that both corrosion current and corrosion potential of alloys depend strongly on the applied sress, the increasing of i_{corr} was caused by the deformation. Gutman et al. [29] found that the anodic polarization curves are changed within the nonlinear region under the mechanical action manifesting the mechanochemical effect (the influence of deformation on anodic polarization) Zhang et al.[30] thought that applied stress enhances anodic dissolution of the steel. The polarization current density, I_d, corresponding to the corrosion potential E could be obtained from the polarization curves, for example, I_d is 0.0023A/cm^2 when E is -0.459V (under the condition of T_S is 0MPa and D_I is 0.5mA/cm^2). Table 5 shows the polarization current density of X80 steel in Daqing solution under different tensile stress. Base on the above conditions, we can calculate the corrosion rate. According to Faraday law, the quality participate in the electrode reaction is proportional to current intensity and conduction time through the electrolyte in the electrolysis process, the quality participate in the electrode reaction is only proportional to chemical equivalent of this substance if the electrode through the same electric quantity. Above process can be shown by the following equations:

$$m = k \cdot Q = k \cdot I \cdot t \qquad (1)$$

$$K = \frac{M}{F \cdot n} \qquad (2)$$

Where, m is the quality participate in the electrode reaction, kg; k is constant of proportionality (electrochemical equivalent); Q is electric quantity, C; I is current intensity, A; t is conduction time, s; K is electrochemical equivalent of reactive substances; M is molar mass of reactive substances, kg/mol; F is the Faraday constant, 96485C/mol; n is the valence of metal ions.

The specimen corrosion rate can be calculated by the following equation:

$$v = \frac{m}{A \cdot t} \qquad (3)$$

Where, v is corrosion rate, $g/cm^2 \cdot h$; A is exposed surface area of specimen, cm^2; t is corrosion time, h.

Synthetic Eqs. 1-3, the relationship between the polarization current density and corrosion rate can be obtained:

$$v = \frac{M \cdot I_d}{F \cdot n} \quad (4)$$

Known, I_d =0.0023 A/cm^2, M=56g/mol, n=2, therefore, $v \approx 2.4\times10^{-3} g/cm^2 \cdot h$ can be calculated according to eq. 4. Similarly, the corrosion rate under other current density can be calculated (as shown in Table 6).

Table 5. The polarization current density of X80 steel in Daqing solution under different tensile stress.

Ts (MPa)	0.5 mA/cm^2	1.0 mA/cm^2	1.5 mA/cm^2	2.0 mA/cm^2	2.5 mA/cm^2	3.0 mA/cm^2	3.5 mA/cm^2
0	0.0023	0.0046	0.0069	0.0092	0.0115	0.0139	0.0160
165.5	0.0024	0.0048	0.0071	0.0095	0.0119	0.0144	0.0167
273	0.0025	0.005	0.0073	0.0097	0.0123	0.0147	0.017
441.6	0.0027	0.0053	0.0075	0.01	0.0126	0.0149	0.0173
552	0.0036	0.0063	0.0092	0.0118	0.0145	0.0169	0.0195

Table 6. DC stray current-induced corrosion rate of X80 steel in Daqing solution under different tensile stress.

Ts (MPa)	0.5 mA/cm^2	1.0 mA/cm^2	1.5 mA/cm^2	2.0 mA/cm^2	2.5 mA/cm^2	3.0 mA/cm^2	3.5 mA/cm^2
0	0.0024	0.0048	0.0072	0.0096	0.0120	0.0145	0.0167
165.5	0.0025	0.0050	0.0074	0.0099	0.0124	0.0150	0.0175
273	0.0026	0.0052	0.0076	0.0101	0.0129	0.0154	0.0178
441.6	0.0028	0.0055	0.0078	0.0105	0.0132	0.0156	0.0181
552	0.0038	0.0066	0.0096	0.0123	0.0152	0.0177	0.0204

According to Table 3, the relation curve (as shown in Fig. 9) between stray current density and potential under different stress states can be drown. It is seen that the corrosion rate of X80 steel increases gradually as the stress and stray current density increase from Fig. 9, the effect of tensile stress on the corrosion rate became increasingly apparent with the increase of stray current density. During elastic deformation, with the increase of tensile stress, corrosion potential of X80 pipeline steel is small amplitude declining, while, the corrosion potential is small amplitude rising; Mutation in corrosion potential and corrosion rate appeared when plastic deformation take place in X80 pipeline steel, while, the relationships between corrosion potential, corrosion rate and stress are all unlinear.

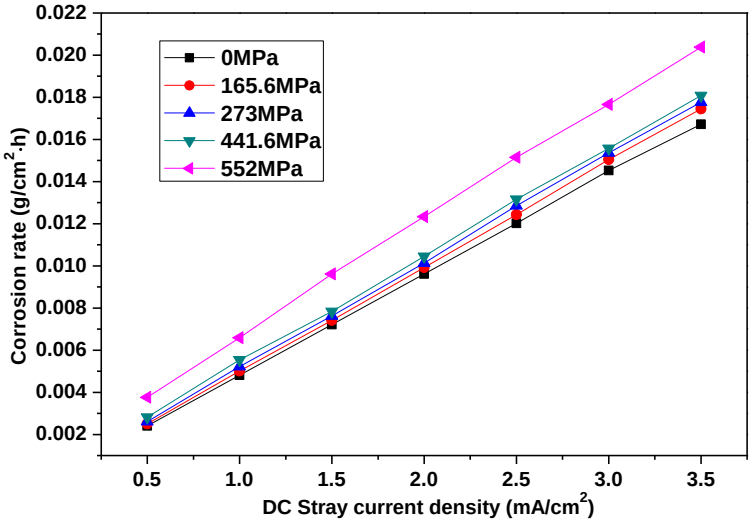

Figure 9. The relation curve between corrosion rate and DC stray current density of X80 pipeline steel in Daqing solution under different tensile stress levels.

3.4. Corrosion morphology

Fig. 10 shows macro corrosion morphology and local (a), (b) enlarging images of X80 steel when D_I is 2.0mA/cm^2, Ts is 441.6MPa.

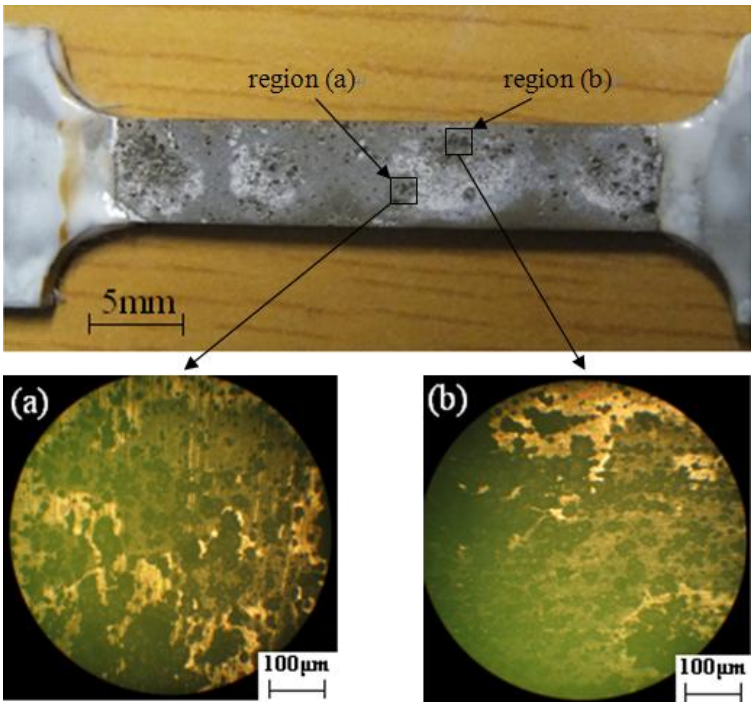

Figure 10. Macro corrosion morphology and local (a), (b) enlarging images of specimen in Daqing solution when D_I is 2.0mA/cm^2,Ts is 441.6MPa.

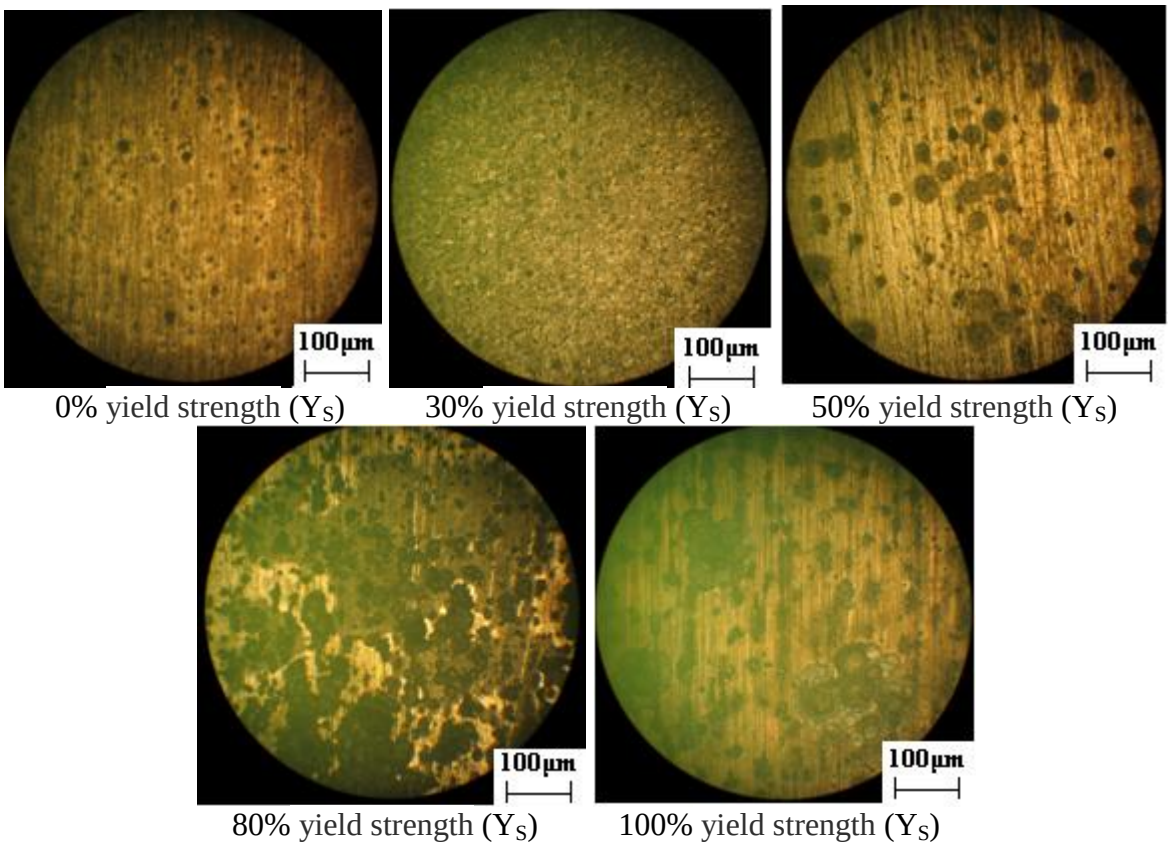

Figure 11. Corrosion morphology images of X80 pipeline steel in Daqing solution when D_I is 2.0mA/cm^2.

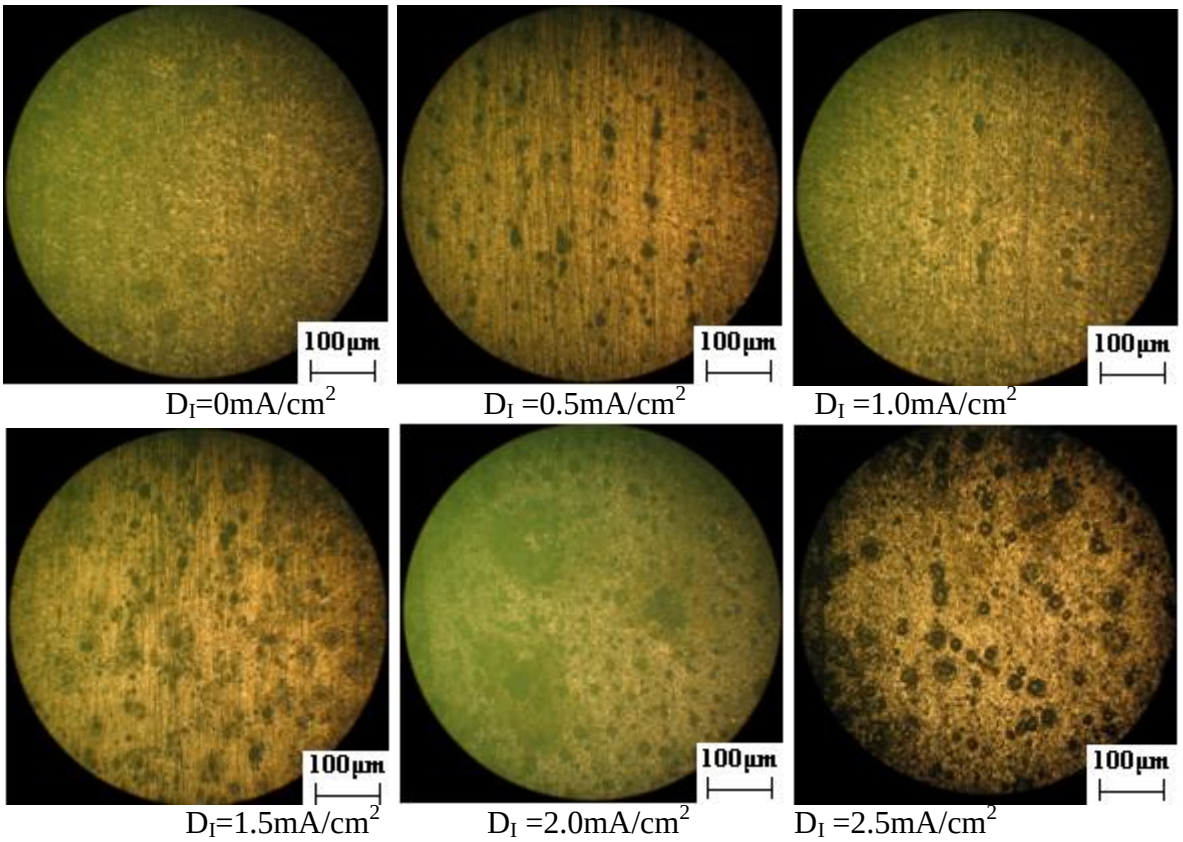

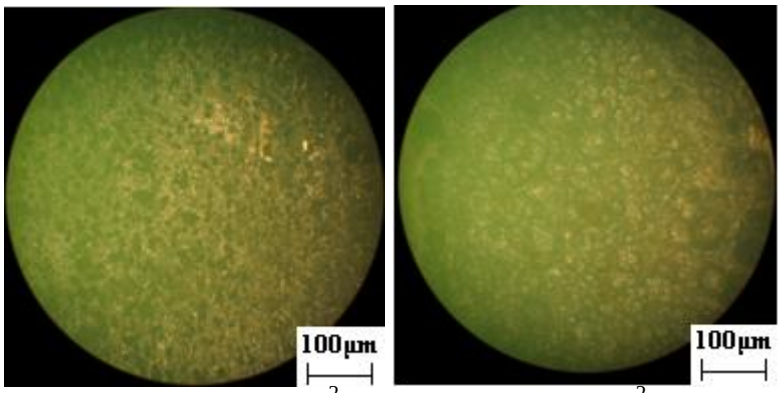

D_I =3.0mA/cm^2 D_I =3.5mA/cm^2

Figure 12. Corrosion morphology images of X80 pipeline steel in Daqing solution when T_S is 276 MPa.

Using microscope to observe the specimens after corrosion, and then select the corrosion morphology amplification (X100) figures of the same region (a). We select the corrosion morphology images (as shown in Fig. 11) when D_I is 2.0mA/cm^2, and select the corrosion morphology images (as shown in Fig. 12) when T_S is 276 MPa.

Zhang et al.[30] thought that when the local stress concentration is not significant enough to approach the yielding strength of the steel, the steel is still in arelatively stable state, and there is a uniform distribution of dissolution rate over the whole surface of the steel specimen. As shown in Figs. 11 and 12, the uniform corrosion is occurred on X80 pipeline steel surface, as the stress enhance, the quantity of etch pits in unit area and the etching depth increase negatively, indicate that the applied stress enhance the corrosion activity, furthermore, the etch pit density, diameter and depth increase negatively with the increase of stray current density. It is demonstrated that corrosion rate of steel increase mainly reflect in the increase of etch pit density, diameter and depth combined with Figs. 10-12.

4. DISCUSSION

According to the mechanochemical interactions theory of Gutman [31-33] and other related studies [22, 23, 26-30,34-35], The external work will affect thermal potential of the reaction system when the electrode subject the effect of the applied stress in electrochemical reaction, in single cation system under the simultaneous action of mechanical and electrical elements, the cation electrochemical bit can be expressed by:

$$\bar{\mu} = \mu_0 + RT\ln a + \Delta PV_m + zF\varphi = \mu_0 + RT\ln \bar{\bar{a}} \qquad (5)$$

Wherein,

$$\bar{\bar{a}} = a \cdot \exp\frac{zF\varphi + \Delta PV_m}{RT} \qquad (6)$$

Where, $\bar{\mu}$ is the electrochemical bit after electrode force, μ_0 is anode metal standard chemical potential, R is the gas constant, T is absolute temperature, ΔP is applied stress, V_m is molar volume of the steel, z is anode valence, F is the Faraday constant, φ is anode metal potential, a is anode metal thermodynamic activity，$\bar{\bar{a}}$ is anode metal mechanochemical activity.

During macro elastic deformation, an external load (ΔP >0) would decrease the change of electrode potential ($\Delta\varphi_e^0$) of X80 steel and enhance its corrosion activity according Eq. 5 when the thermodynamic potential Δu is very small ($\Delta u \to 0$), $\Delta\varphi_e^0$ can be given by:

$$\Delta\varphi_e^0 = -\frac{\Delta P V_m}{zF} \qquad (7)$$

$\Delta\varphi_e^0$ decreases gradually as the stress increases, which leads to the open circuit potential in Fig. 4, the negative anodic polarization curves in Fig. 8, the potential under different DC stray current density in Fig. 6 all shifted negatively, and the relationship in Fig. 7 between stress and corrosion potential is linear. Since the corrosion potential in Fig. 8 correlates positively with the polarization current, therefore, there is a linear relationship between the corrosion rate and stress based on Faraday law. The above analysis is consistent with test results.

When the strain reaches plastic deformation, the change of electrode potential, $\Delta\varphi_p^0$, can be calculated by:

$$\Delta\varphi_p^0 = -\frac{TR}{zF}\ln\left(\frac{\upsilon\alpha}{N_0}\varepsilon_p + 1\right) \qquad (8)$$

Wherein,

$$\varepsilon_p = \frac{N_0}{\alpha\upsilon}\left[\exp\left(\frac{n\Delta\tau}{\alpha k N_{\max} T}\right) - 1\right] \qquad (9)$$

Where, N_0 is the initial density of dislocations prior to plastic deformation, υ is the orientation-dependent factor, equalling to 0.4-0.5 for tensile deformation, α is a coefficient of 10^9 —$10^{11} cm^{-2}$, ε_p is plastic strain, n is the number of dislocations in a dislocation pile-up, $\Delta\tau$ is the hardening intensity, $N_{\max}$ is the maximum dislocation density, k is the Boltzmann constant. In this case, electrode potential of X80 steel continues to decline and the relationship between the change of electrode potential and stress is changed from linear to logarithmic, so corrosion potential will produce a significant mutation, which leads to the open circuit potential in Fig. 5, the negative anodic polarization curves in Fig. 8, the potential under different DC stray current density in Fig. 7 rapid decline. Similarly, the mutation in corrosion potential leads to the mutation of corrosion rate according to Faraday law, which explains the results in Fig. 9.

In present work, anodic dissolution current density i of specimen experiencing both elastic and plastic deformation stages is determined by [33]:

$$i = i_a\left(\frac{\upsilon\alpha}{N_0}\varepsilon_p + 1\right)\exp\left(\frac{\Delta P_m V_m}{RT}\right) - i_c \qquad (10)$$

Where, i_a and i_c refer to current density of anodic and cathodic respectively, ΔP_m is excess pressure to elastic deformation limit that is equal to 1/3 of yield strength of X80 steel. Assume that the external stress on the specimen does not affect the ion activity in Daqing solution, i_c remains constant.

It is thus apparent that the anodic dissolution rate of the steel is accelerated by external stress/strain [32] . In elastic deformation, i only has a small increase , however, it has a significant mutation in plastic stage as a rapid increase of i_a . According to Eq. 4, the above changes of i will lead to the same changes of corrosion rate. It is similar to the above analysis, and the accuracy of experimental results is further proved. In summary, we can see that DC stray current-induced corrosion of X80 pipeline steel is accelerated with the increase of stress.

In elastic deformation region, a mathematical relationship between corrosion rate C_r and Y_s, D_I was obtained through multiple linear regression:

$$C_r = -5.0\times10^{-4} + 5\times10^{-3} D_I + 1.1\times10^{-3} Y_s \qquad (11)$$

Upon examination, the significance and precision of Eq. 11 meet the requirement. It is seen that the effect of latter on corrosion rate of X80 pipeline steel is more significant when only considering two factors of stress and stray current density during elastic deformation.

5. CONCLUSIONS

The following conclusions can be made based on the results presented in the paper.

a) The polarization curve, corrosion potential with and without superimposed DC stray current of X80 pipeline steel all shift negatively, and the corrosion rate increase with the enhancement of tensile stress in Daqing (alkaline) solution. Moreover, the above laws become increasingly apparent with the increase of stray current density.

b) In elastic deformation region, the relationships between stress and corrosion potential, corrosion rate of X80 pipeline steel are approximately linear. Mutation in corrosion potential and corrosion rate appear when the plastic deformation take place in X80 pipeline steel, while, the relationships between stress and corrosion potential, corrosion rate are all unlinear.

c) The corrosion rate increase mainly reflects in the increase of etch pit density, diameter and depth on X80 pipeline steel surface.

d) During elastic deformation, compared with the stress, the effect of stray current density on corrosion rate of X80 pipeline steel is more significant.

ACKNOWLEDGEMENT
This work was supported by National High Technology Research and Development Program of China (No. 2012AA040105).

References

1. M. Hudson, *PhD thesis*, Cranfield University, UK (2004).
2. F. Mohammadi, F. F. Eliyan, Akram Alfantazi, *Corros. Sci.* 63 (2012) 323.
3. A. B. Forero, J. A. C. Ponciano, I. S. Bott, *Mater. Corros.* 63 (2012) 9999.
4. G. M. Omweg, G. S. Frankel, W. A. Bruce, G. Koch, *CORROSION.* 2 (2002) 48.

5. M. Ueda, T. Omura, S. Nakamura, T. Abe, K. Nakamura, P. I. Nice, J. W. Martin, *CORROSION*. 5 (2005) 89.
6. S. Y. Shin, B. Hwang, Lee S, *Mater. Sci. Eng.A.* 458 (2007) 281.
7. F. R. Xiao, B. Liao, Y. Y. Shan, *Mater. Sci. Eng.A.* 431 (2006) 41.
8. T. Janzen, W. N. Horner, presented at *Proc. Int. Conf. on Pipeline*, ASME, USA 1998, pp. 83–88.
9. B. Tanguy, T. T. Luu, G. Perrin, *Int. J. Pres. Ves. Pip*. 85 (2008) 322.
10. Zhou J, Horsley D, Rothwell B, *Proc. the 7th Inter. Pipeline Conf*, ASME, Canada 2006 (paper no. 2006-10054).
11. H. Arslan, J. Hamilton, S Lele, *Proc. the 8th Inter. Pipeline Conf*, ASME, Canada 2010, (paper no. 2010-31505).
12. G. V. Boven, W. Chen, R. Rogge, *Acta. Mater.* 55 (2007) 43.
13. X. Tang, Y. F. Cheng, *Electrochim. Acta.*54 (2009) 1499.
14. G. A. Zhang, Y. F. Cheng, *Corros. Sci.* 52 (2010) 960.
15. The Danish Gas Technological Centre, *Report of AC / DC interference corrosion in pipelines*, MetriCorr, Denmark (2006).
16. E. Collet, B. Delores, M. Gabillard, *Anti-Corros. Method. M.* 48 (2001) 221.
17. S. Muralidharan, D. K. Kim, T. H. Ha, J. H. Bae, Y. C. Ha, H. G Lee, J.D. Scantlebury, *Desalination.* 216 (2007) 103.
18. D. K. Kim, S. Muralidharan, T. H. Ha, J. H. Bae, Y. C. Ha, H. G. Lee, J.D. Scantlebury, *Electrochim. Acta.* 51 (2006) 5259.
19. A.Q. Fu, Y. F Cheng, *Corros. Sci.* 52 (2010) 612.
20. L. Y. Xu, X. Su, Z. X. Yin, *Corros. Sci.* 61 (2012) 215.
21. F. Hasan, J. Iqbal, F. Ahmed, *Eng. Fail. Anal.* 14 (2007) 801.
22. Y. X .Wang, W. M. Zhao, H. Ai, *Corros. Sci.* 53 (2012) 2761.
23. R. K. Ren, S. Zhang, X. L. Pang, *Electrochim. Acta.* 85 (2012) 283.
24. L. Y. Xu, Y. F. Cheng, *Corros. Sci.* 59 (2012) 103.
25. S. X. Rao, L. Q. Zhu, D. Li, *J. Chin. Soc. Corros. Prot.* 27 (2007) 228.
26. L. Y. Xu, Y. F. Cheng, *Corros. Sci.* 64 (2012) 145.
27. L. Y. Xu, Y. F. Cheng, *Corros. Sci.* 73 (2013) 150.
28. P. L. Bonora, M. Andrei, A. Eliezer, *Corros. Sci.* 44 (2002) 729.
29. E. M. Gutman, G. Solovioff, D. Eliezer, *Corros. Sci.* 38 (1996) 1141.
30. C. Zhang and Y.F. Cheng, *J. Mater. Eng. Perform.* 19 (2010) 1284.
31. E. M. Gutman, *Mechanochemistry and corrosion prevention of metals.* Science Publication, Peking (1989).
32. E. M. Gutman, *Mechanochemistry of solid surfaces*. World Scientific Publication, Singapore (1994).
33. E. M. Gutman. *Mechanochemistry of Materials*. Cambridge Interscience Publishing, Cambridge (1998).
34. X. H. Wang, C, X, Yin, J. D. Wang. *J. Chin. Univ. Petr.* 37 (2013) 119.
35. D. H. Dan, G. H. He, *J. South. Jiaotong. Univ.* 36 (2001) 181.